Polymer Journal (2016) 48, 1123–1131

www.nature.com/pj

ORIGINAL ARTICLE

Complete and comprehensive orientation of cylindrical microdomains in a block copolymer sheet

Shogo Tomita, Hiroshi Urakawa, Isao Wataoka, Sono Sasaki and Shinichi Sakurai

Significant progress in cylindrical microdomain orientation is reported for a polystyrene-*block*-poly(ethylene-*co*-butylene)-*block*-polystyrene triblock copolymer (SEBS-16) as analyzed by two-dimensional small-angle X-ray scattering. For this purpose, the morphological transition from sphere to cylinder was utilized. By applying compressional flow to the SEBS-16 specimen undergoing a morphological transition at 210 °C, superior cylinder orientation was achieved compared with the results obtained by applying the compressional flow to a cylindrical phase. The flow-treated specimens were further subjected to subsequent thermal annealing at 210 °C. It was found that the cylinder orientation proceeded by the subsequent thermal annealing even for flow-treated specimens with less oriented cylinders. Furthermore, the fraction of grains in which the $(10\bar{1}0)$ plane of the hexagonal lattice of cylinders is oriented parallel to the specimen surface increased due to the subsequent thermal annealing, even for the specimen with the best cylinder orientation.
Polymer Journal (2016) **48,** 1123–1131; doi:10.1038/pj.2016.83; published online 5 October 2016

INTRODUCTION

The control of self-assembled structures formed in block copolymers has attracted a great deal of research interest, largely because of the novel physical properties expected to arise from well controlled microdomain structures, including spheres, cylinders, double-gyroids and lamellae. It is well known that the morphology of the microdomain structure can be thermodynamically controlled by careful manipulation of parameters, including the volume fractions of each block component, temperature, and the molecular weight of block copolymers.[1–8] The morphology can also be altered and kinetically locked in for an as-cast sample by using a selective solvent to prepare the polymer solution for the solution casting process.[9–13]

One of the unique characteristics of block copolymers is the ability to exhibit anisotropic physical properties, generated by orienting microdomains with anisotropic shapes, such as cylinders or lamellae. For example, with glassy cylinders embedded in a rubbery matrix, if cylinders are oriented perpendicular to the surface of the film, the film possesses the anisotropic physical property of being hard to compress but easy to stretch in any direction parallel to the film surface. Nanochannels piercing through the film can be created in this case, and these films can be applied as templates for magnetic recording devices. Therefore, a significant amount of effort is directed towards achieving perpendicularly oriented cylinders using any of the numerous reported methods.[14–23] Among these reports, Karim *et al.* demonstrated that so-called cold zone annealing is able to perpendicularly orient cylinders.[20,21] The cold zone annealing method specifically utilizes a temperature gradient with the maximum temperature below the order–disorder transition temperature. Notably, the withdrawal speed of the substrate crossing the temperature-gradient zone was key for obtaining a high proportion of perpendicularly oriented cylinders. Xu *et al.* showed that the application of an electric field with sufficiently high voltage (40 V mm^{-1}) to a polystyrene-*block*-poly(methyl methacrylate) diblock copolymer thin film, which forms spherical microdomains at room temperature, can induce a sphere-to-cylinder transition even at room temperature, aligning the thus-formed cylinders perpendicularly to the film surface.[17] In our previous research, we showed that a perpendicular orientation of cylindrical microdomains resulted from thermally annealing a polystyrene-*block*-poly(ethylene-*co*-butylene)-*block*-polystyrene (SEBS-16) triblock copolymer film, first forming non-equilibrium spheres that then coalesced in a preferentially perpendicular direction to the film surface; following this procedure, perpendicularly oriented cylinders were obtained.[19]

In addition, many researchers are interested in forming cylinders parallel to the film surface due to the potential applications as templates for patterned surfaces with spacing on the order of 10 nm. Mansky *et al.* first proposed reactive ion etching as a fabrication method for patterned surfaces by exposing block copolymer thin films to ionized gas, which results in different etching rates for each block component.[24] In block copolymer films with uniaxially oriented cylinders parallel to the direction of flow, anisotropic mechanical properties are seen, particularly for films with glassy cylinders embedded in a rubbery matrix phase.[25–28] In addition, anisotropies in heat flow, ion transportation, electric conductivity, or other properties are also achieved in these films. A variety of methods has been proposed to align anisotropic microdomains parallel to the film surface, including applying compressional flow[25,26] or shear flow.[29–36]

Department of Biobased Materials Science, Kyoto Institute of Technology, Matsugasaki, Sakyo-ku, Kyoto, Japan
Correspondence: Professor S Sakurai, Department of Biobased Materials Science, Kyoto Institute of Technology, Matsugasaki, Sakyo-ku, Kyoto 606-8585, Japan.
E-mail: shin@kit.ac.jp
Received 21 June 2016; revised 8 August 2016; accepted 8 August 2016; published online 5 October 2016

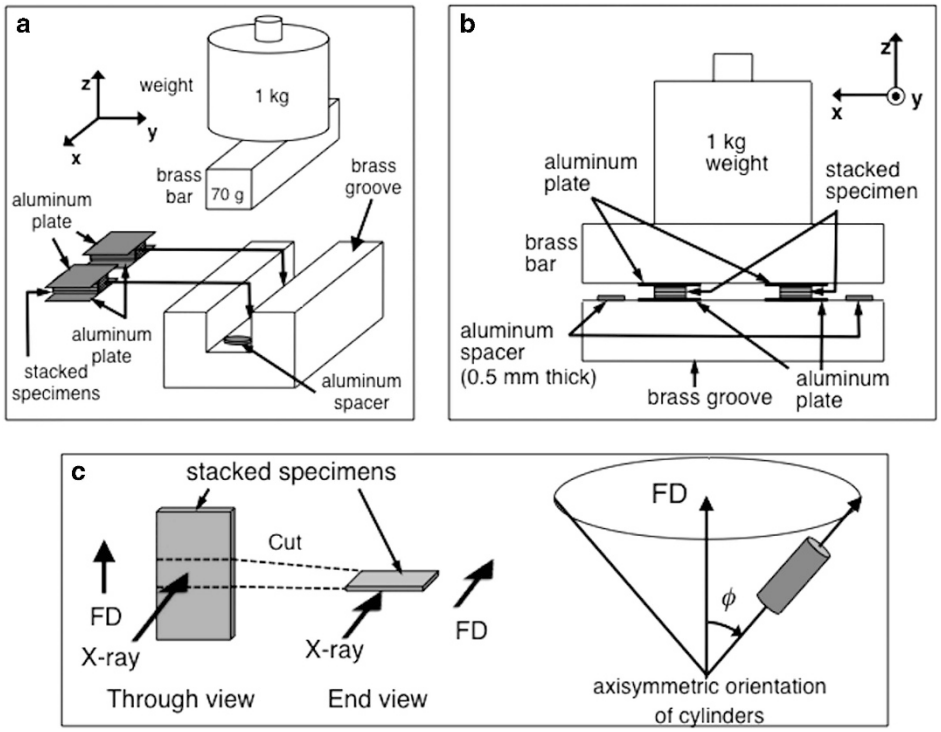

Figure 1 (**a**, **b**) Schematic illustrations of the fixture to apply a flow field to stacked specimens. (**c**) Schematic illustration showing the axisymmetric orientation of cylinders with respect to FD (flow direction) and the geometry of the stacked specimens for the SAXS measurement (through and end view).

In this paper, we present an appreciably high degree of parallel oriented cylinders through utilization of non-equilibrium sphere coalescence in a SEBS-16 triblock copolymer film. Notably, this technique is also able to produce cylinders with a perpendicular orientation.[19] When a flow is applied to the sample, the expectation is that a superior orientation of cylinders parallel to the flow-direction (FD) will be obtained compared with the application of flow directly onto cylinders. In the latter case, a partial break-up and reconnection of the pinched cylinders may be required, for which a large activation energy would be necessary. For samples to which a flow is applied, a high strain may be necessary to obtain highly oriented cylinders. Specifically, a strain as high as 10 has often been applied in the literature.[25,26] By contrast, in our method, a strain of 1.5–4.5 was high enough to achieve highly oriented cylinders. The load used for applying flow was low because a slow deformation of the specimen was considered to be favorable for cylinder orientation. As a result, a prolonged time was required for the application of the flow. It should be noted here that the strain was accordingly increased with an increase of the annealing time (from 30 to 120 min). In other words, our method (see Figure 1 in detail) cannot independently control applied strain. However, in this study, our aim was to demonstrate the superiority and simplicity of using a compression flow with a slow deformation rate for cylindrical orientation. As a result, both a high degree of cylinder orientation parallel to FD and the most favorable hexagonal lattice orientation, an orientation of the $(10\bar{1}0)$ planes parallel to the specimen surface, were obtained.

EXPERIMENTAL PROCEDURE

Sample

SEBS-16 was used; the molecular characteristics were $M_n = 6.6 \times 10^4$ and $M_w/M_n = 1.03$, where M_n and M_w denote number-averaged and weight-averaged molecular weights, respectively, and a polystyrene (PS) volume fraction of 0.16. Two types of solutions were prepared. First, a selective solvent, *n*-heptane, was used which was a poor solvent for PS and a good solvent for poly(ethylene-*co*-butylene) (PEB). We note that dichloromethane, which is a selectively good solvent for PS, was used as a co-solvent to obtain complete solubilization, as it was not possible to dissolve the SEBS-16 specimen with only *n*-heptane. As the dichloromethane quickly evaporated, the SEBS-16 solution in *n*-heptane was obtained during an early stage of solution casting. Subsequently, the remaining *n*-heptane gradually evaporated. Second, the common solvent, toluene, was used in solution preparation. In either case, the polymer concentration was 5.0 wt%. The selective solvent *n*-heptane was used to form a non-equilibrium morphology (spheres) with the potential to transition to a thermodynamically equilibrium state (cylinders) by thermally annealing the sample at a temperature sufficiently higher than the glass-transition temperature (Tg) of PS, which was determined to be 54.8 °C using a differential scanning calorimeter (see Supplementary Figure S1 in the supporting information). In our previous work, we found that the spontaneous orientation of cylinders perpendicular to the film surface occurred by thermally annealing the SEBS-16 film, which was prepared with a selective solvent.[19] The SEBS-16 film, which had a thickness of 0.3 mm, was prepared by completely evaporating the solvents from either solution at room temperature.

Application of compressional flow

To impose a compressive flow on the as-cast specimens, we utilized a channel-cut die and a bar made of copper, shown schematically in Figure 1.[37] This apparatus induces a flow in a polymeric film, of which concept was originally proposed by Khan and Larson.[38] However, our apparatus more closely resembles the design by Lee *et al.*[25] As-cast films were cut into rectangular pieces with dimensions 3×10 mm and then stacked to a total thickness of ~2.0 mm. The stack of as-cast films was sandwiched between two pieces of aluminum, with each aluminum plate having a thickness of 0.1 mm. The width of the film and the aluminum plates had to fit exactly into the die to induce the one-dimensional flow field parallel to the die groove. Several drops of silicone oil (Momentive Performance Materials Co., Ltd., Waterford, NY, USA) were placed on the film surface to avoid a shearing effect on the specimen. Then, a rigid bar (70*g*) was put on top of two side-by-side sets of the stacked films,

which were both sandwiched between aluminum plates, and an additional weight of 1 kg was placed on the bar. The whole setup, including the die, the bar, and the stacked films, was put into an oven filled with nitrogen gas. When the temperature was elevated above the Tg of PS, the films softened and the bar moved down. Hereafter, the thermal annealing process for the stacked films using a load is referred to as the 'preannealing process.' The rationale for using two sets of stacked films was to balance the bar during its displacement. The 1 kg weight was chosen to impose an appropriate displacement rate for inducing orientation; it is well known that a high strain is useful for aligning cylindrical microdomains parallel to the flow.[39] We note that the displacement distance can be increased by prolonging thermal annealing. The final thicknesses of the stacked specimens did not reach the spacer thickness (0.5 mm) even after 120 min of preannealing at 210 °C. Furthermore, the extent of flow changed slightly between samples, even for the same preannealing conditions (temperature/duration). Thus, the extent of flow was characterized for each specimen by the compressional strain ε, which is defined by the thicknesses of the stacked films before and after preannealing, d_0 and d, respectively, as follows:

$$\varepsilon = \frac{d_0 - d}{d_0} \tag{1}$$

Table 1 Preparation conditions for specimens

Specimen Code	*Preannealing condition*	*Compressional strain ε*	*Subsequent thermal annealing (without loading)*	*Cast solvent*
Hep-1	210 °C/3 h	0	—	*n*-heptane
Hep-2,3,4	140 °C/60 min	1.49–1.66	—	"
Hep-2a	"	1.61	210 °C/10 min	"
Hep-3a	"	1.66	210 °C/30 min	"
Hep-4a	"	1.49	210 °C/60 min	"
Hep-5,6,7	140 °C/ 120 min	2.24–2.78	—	"
Hep-5a		2.60	210 °C/10 min	"
Hep-6a		2.78	210 °C/30 min	"
Hep-7a		2.24	210 °C/60 min	"
Hep-8	210 °C/30 min	1.81	—	"
Hep-8a	"	"	210 °C/10 min	"
Hep-8b	"	"	210 °C/30 min	"
Hep-8c	"	"	210 °C/60 min	"
Hep-9	210 °C/60 min	2.90	—	"
Hep-9a	"	"	210 °C/10 min	"
Hep-9b	"	"	210 °C/30 min	"
Hep-9c	"	"	210 °C/60 min	"
Hep-10	210 °C/ 120 min	4.51	—	"
Hep-10a	"	"	210 °C/10 min	"
Hep-10b	"	"	210 °C/30 min	"
Hep-10c	"	"	210 °C/60 min	"
Tol-1	210 °C/30 min	2.00	—	Toluene
Tol-1a	"	"	210 °C/10 min	"
Tol-1b	"	"	210 °C/30 min	"
Tol-1c	"	"	210 °C/60 min	"
Tol-2	210 °C/60 min	3.84	—	"
Tol-2a	"	"	210 °C/10 min	"
Tol-2b	"	"	210 °C/30 min	"
Tol-2c	"	"	210 °C/60 min	"

The entire setup, which included the die, the bar, and the stacked films, was quenched in ice water after the predetermined annealing time was completed. The preannealing conditions (temperature/duration and ε) for all specimens are summarized in Table 1, where Hep and Tol in the specimen code stand for *n*-heptane and toluene, which were used as the casting solvent.

In our previous study (Shiho & Sakurai, unpublished results), it was revealed that cylinder orientation was largely determined by subsequent thermal annealing of the preannealed specimen for specimens in which cylindrical microdomains were directly aligned by the flow. Therefore, in the current study we evaluated the same procedure to ensure its significance. The subsequent thermal annealing was conducted at 210 °C for 10, 30 or 60 min under a nitrogen atmosphere without a load for preannealed films, which were removed from the mold. For the Hep-8–10 and Tol-1–2 specimens, changes in orientation were examined using single preannealed specimens by conducting step-by-step subsequent thermal annealing at a given temperature.

2d-SAXS measurement

Two-dimensional small-angle X-ray scattering (2d-SAXS) measurements were performed to analyze the cylinder orientation. We used a Nano-Viewer (RIGAKU Co., Ltd., Akishima, Tokyo, Japan) composed of a rotating-anode X-ray generator with an electron gun consisting of a tungsten filament, a Osmotic Confocal Max Flux Mirror (CMF, Rigaku Co., Ltd.) for focusing the X-ray beam, three collimation pinhole slits (0.7, 0.8 and 0.8 mmϕ for the first, second and third slits, respectively) for adjusting the beam size and removing parasitic scattering, a vacuum chamber, and a two-dimensional detector (PILATUS 100K, DECTRIS Ltd., Baden, Switzerland). The wavelength components other than CuKα (wavelength $\lambda = 0.154$ nm) were eliminated using a Ni filter. The sample-to-detector distance was set to 1.0 m. The focal length of the CMF mirror was 900 mm and the distance from the mirror to the 2d-detector (PILATUS) was 2000 mm in the Rigaku NANO-Viewer SAXS collimation; therefore, the X-ray beam on the 2d-detector was defocused. Therefore, the measured 2d-SAXS patterns were smeared. However, the extent of smearing was considered to be trivial such that desmearing of the 2d-SAXS pattern was not conducted. Any unfavorable effects due to smearing on the data analyses (determination of values such as the orientation factor and the peak intensity fraction, as discussed below) were also considered to be trivial.

As a result of applying a flow to the specimens, the cylinders were oriented with respect to FD; the resulting axisymmetric orientation of the cylinders is shown schematically in Figure 1c. Because the extent of cylinder orientation was the highest at the front of the specimen, which we will discuss in a future publication, the front part of the specimen was analyzed by a 2d-SAXS measurement with the X-ray irradiation normal to the film (hereafter referred to as the 'through view') at room temperature, as shown schematically in Figure 1c. After the through view 2d-SAXS measurements, the film specimens were cut to a dimension of 2 mm along FD and further 2d-SAXS measurements were conducted at room temperature with the incident X-ray beam irradiation parallel to the FD (hereafter referred to as the 'end view'), shown schematically in Figure 1c.

RESULTS AND DISCUSSION

First of all, one can confirm that perpendicularly oriented cylinders were formed upon coalescence of the non-equilibrium spheres by thermal annealing of the as-cast sample (from *n*-heptane solution) without application of flow in Figure 2 where the 2d-SAXS pattern (edge view) for Hep-1 is shown. Note that the edge view 2d-SAXS pattern was measured by illuminating X-ray from the direction perpendicular to the normal ($\boldsymbol{n}$) of the specimen surface (not the case as shown schematically in Figure 1c), where q represents the magnitude of the scattering vector:

$$q = \frac{4\pi}{\lambda} \sin\frac{\theta}{2} \tag{2}$$

with θ being the scattering angle.

The SAXS pattern in Figure 2 exhibits the anisotropic feature that all reflections appear in an equatorial direction. Since the equatorial

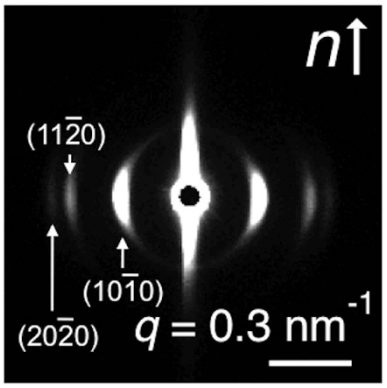

Figure 2 2d-SAXS pattern for Hep-1 by X-ray illumination perpendicular to the normal of the film surface (***n***).

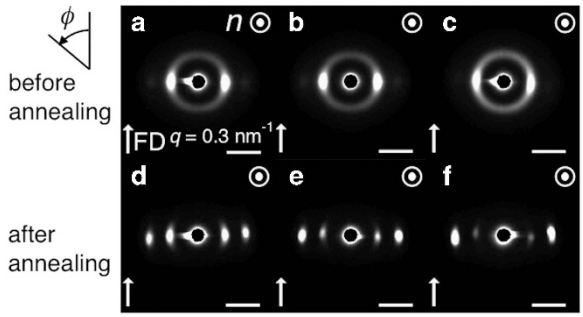

Figure 3 2d-SAXS patterns (through view) measured for (**a**–**c**) Hep-2–4, and (**d**) Hep-2a, (**e**) Hep-3a and (**f**) Hep-4a. In **a**, the definition of the azimuthal angle ϕ is shown.

direction is perpendicular to the specimen normal ***n***, the stated fact above indicates that the cylinders are oriented perpendicular to the specimen surface, confirming that without the application of any flow, the heptane as-cast film produces perpendicularly orientated cylinders.[19]

In the following sections, the orientation of cylinders obtained by applying a flow to the heptane as-cast film is discussed. Figure 3a–c show the 2d-SAXS patterns measured for Hep-2, 3 and 4, respectively, and Figure 3d–f represent Hep-2a, 3a and 4a, respectively. All of the SAXS patterns have spots in the q-direction perpendicular to FD, indicating an orientation of microdomains parallel to FD. To examine the morphology, 1d-SAXS profiles (plots of the scattering intensity as a function of q) were obtained by conducting a sector average from the 2d-SAXS patterns in the meridional or equatorial direction within an azimuthal range of $\pm 10°$. Figure 4 shows the obtained SAXS profiles. Before annealing, all of the equatorial profiles contain two reflection peaks at q positions with q-values assigned to $1:\sqrt{3}$, which are specific to the hexagonal lattice of cylinders. The former and the latter correspond to the $(10\bar{1}0)$ and $(11\bar{2}0)$ reflections, respectively. The morphology of the microdomains formed in the flow-treated sample (before annealing) is no longer spherical but rather cylindrical. In contrast, only a broad peak is seen in the meridional profiles. The disappearance of higher-order peaks may result from a disruption of regularity in the hexagonal symmetry caused by the flow. The existence of the first-order peak in the meridional profile indicates the existence of cylinders oriented perpendicularly to FD, and furthermore this indicates the imperfect nature of orienting cylinders by the application of the flow. It should be noted that the intensity, $I(q^*)$, for the first-order peak is higher than that of the $\sqrt{3}$ peak,

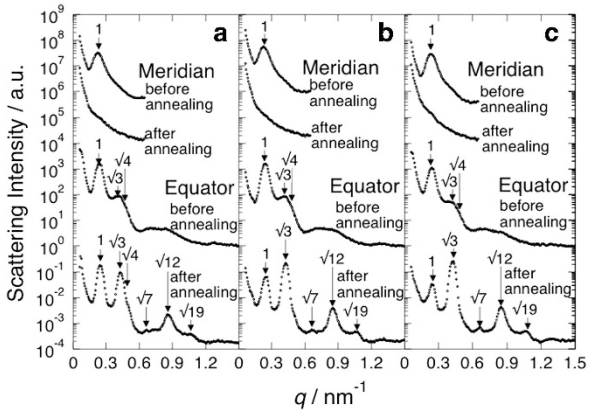

Figure 4 1d-SAXS profiles for the meridional and equatorial directions of the 2d-patterns measured for (**a**) Hep-2/Hep-2a, (**b**) Hep-3/Hep-3a and (**c**) Hep-4/Hep-4a.

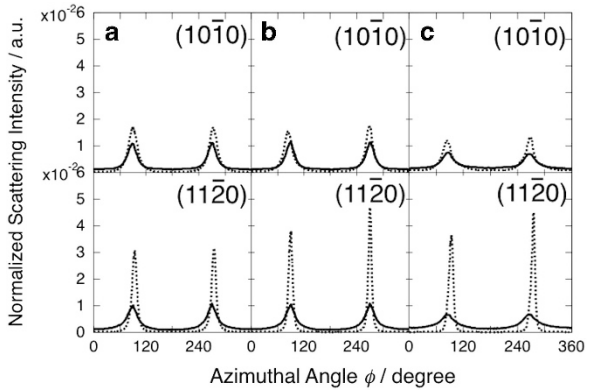

Figure 5 Dependency of intensity on azimuthal angle for $(10\bar{1}0)$ and $(11\bar{2}0)$ reflection peaks for (**a**) Hep-2/Hep-2a, (**b**) Hep-3/Hep-3a, (**c**) Hep-4/Hep-4a, where solid and dotted curves represent before and after the subsequent annealing, respectively.

$I(\sqrt{3}q^*)$, for the specimen without subsequent thermal annealing, and this relationship inverts for the specimen following thermal annealing, as shown in Figures 4b and c. We denote the q value of the first-order peak as q^*. These remarkable changes indicate a preferential orientation of the hexagonal lattice such that the $(10\bar{1}0)$ plane is parallel to the specimen surface, while the $(11\bar{2}0)$ plane is perpendicular to the specimen surface. In this state, the $(10\bar{1}0)$ planes, which contain the largest number of cylinders, are parallel to the specimen surface. Because the densest plane tended to be parallel to the specimen surface, the resulting state of cylindrical orientation was recognized to have the greatest stability. Longer annealing times at 210 °C led to more intense $\sqrt{3}$ peaks, indicating a progression of the $(10\bar{1}0)$ planes parallel to the specimen surface with increasing annealing time.

Figure 5 shows the azimuthal distribution of the scattering intensity for the first-order peak (ascribed to $(10\bar{1}0)$ reflection) and for the $\sqrt{3}$ peak (ascribed to $(11\bar{2}0)$ reflection). The solid and dotted curves represent specimens before and after subsequent thermal annealing, respectively. The azimuthal angle ϕ is defined as shown in Figure 3. In this analysis, the scattering intensity was normalized such that the integrated intensity was set to unity. The peaks at 90 ° and 270 ° for the $(10\bar{1}0)$ and $(11\bar{2}0)$ reflections clearly narrowed with subsequent thermal annealing, indicating an improvement of cylinder orientation parallel to the FD.

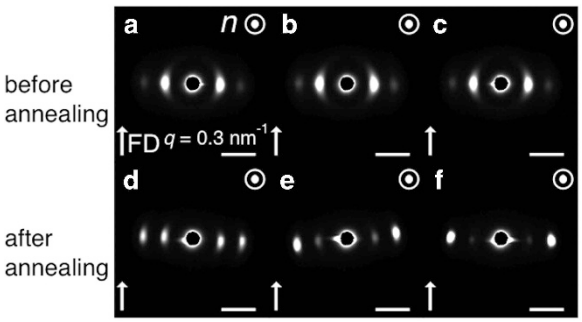

Figure 6 2d-SAXS patterns (through view) measured for (**a**–**c**) Hep-5–7, and (**d**) Hep-5a, (**e**) Hep-6a and (**f**) Hep-7a.

Figure 6a–c show the 2d-SAXS patterns (through view) measured for Hep-5–7, respectively, while Figure 6d–f represent Hep-5a, Hep-6a and Hep-7a, respectively. Compared with the results shown in Figure 3a–c, the 2d-SAXS patterns shown in Figure 6a–c clearly indicate an accumulation of peak intensity in the equatorial direction, indicating that longer preannealing times result in more superior orientation. This superior orientation may be due to the higher degree of compressional strain on the sample (see Table 1). As discussed in Figure 3, the intensity of the $(10\bar{1}0)$ reflection for Hep-6a and 7a weakened in comparison with the $(11\bar{2}0)$ reflection intensity following thermal annealing of Hep-6 and 7. The 1d-SAXS profiles, obtained with the same techniques used to obtain the 1d-profiles in Figure 4, are shown for the meridional and equatorial directions in Figure 7. The first-order peak in the meridional direction for the specimens before the subsequent thermal annealing is much ambiguous as compared with that shown in Figure 4, which is due to the intensity accumulation at $\phi = 90°$ (equatorial direction) by the superior orientation of the cylinders in Hep-5–7. The relative intensity of the $(11\bar{2}0)$ reflection with respect to the $(10\bar{1}0)$ reflection in the equatorial direction before thermal annealing was greater in Figure 7a–c (60 min preannealing) than in Figure 4a–c (30 min preannealing). This result means that the fraction of the grains in which the $(10\bar{1}0)$ planes are parallel to the specimen surface increases with a longer preannealing time. Upon subsequent thermal annealing, the $(11\bar{2}0)$ reflection peak (the $\sqrt{3}$ peak) is clearly observed to be more intense than the $(10\bar{1}0)$ reflection peak (the first-order peak), implying that the phenomenon mentioned above continued with further thermal annealing. This tendency was seen previously in Figure 4.

Figure 8 shows the azimuthal distribution of the scattering intensity, which is similar to the results in Figure 5. However, the width of the peaks appearing at $\phi = 90°$ and 270° for the $(10\bar{1}0)$ reflection seem to be identical before and after subsequent thermal annealing, while the peaks for the $(11\bar{2}0)$ reflection narrowed with subsequent thermal annealing. In principle, the peak width in the azimuthal plot is inversely proportional to the degree of orientation of the plane responsible for the reflection. The fact that the peak width does not change for the $(10\bar{1}0)$ reflection after thermal annealing indicates that the $(10\bar{1}0)$ plane orientation does not appreciably change with respect to FD. In contrast, the experimental results suggest that the orientation of the $(11\bar{2}0)$ plane improved as a result of the subsequent annealing. Initially, the mismatch between orientation behaviors for these planes appears erroneous; however, the reflections originate from different grains. Namely, the observed $(10\bar{1}0)$ reflection is attributed to the grains in which the $(10\bar{1}0)$ planes are perpendicular to the specimen surface, while the observed $(11\bar{2}0)$ reflection corresponds to the grains in which the $(10\bar{1}0)$ planes are parallel to the specimen surface. Therefore, we conclude that the orientation of the former grain was not improved, while the orientation of the latter grain was improved after the subsequent annealing. The finding that the orientation of the grains in which the $(10\bar{1}0)$ planes are perpendicular to the specimen surface was not improved contrasts significantly with the Hep-2–4 (60 min preannealing) results. With close examination, the solid curves in Figure 8 and the dotted curves in Figure 5 for the $(10\bar{1}0)$ reflection seem similar. Therefore, the specimen had already obtained an appreciable orientation after preannealing for 120 min; the subsequent thermal annealing did not contribute to further improvements in orientation. Thus, hereafter we only evaluate the orientation factor for the grain providing the $(11\bar{2}0)$ reflection (the $\sqrt{3}$ peak).

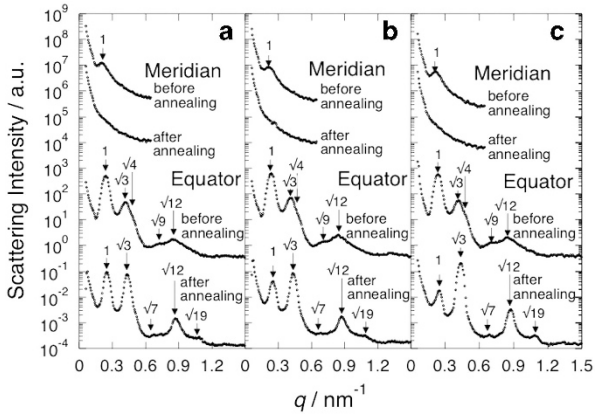

Figure 7 1d-SAXS profiles for the meridional and equatorial directions of the 2d-patterns measured for (**a**) Hep-5/Hep-5a, (**b**) Hep-6/Hep-6a and (**c**) Hep-7/Hep-7a.

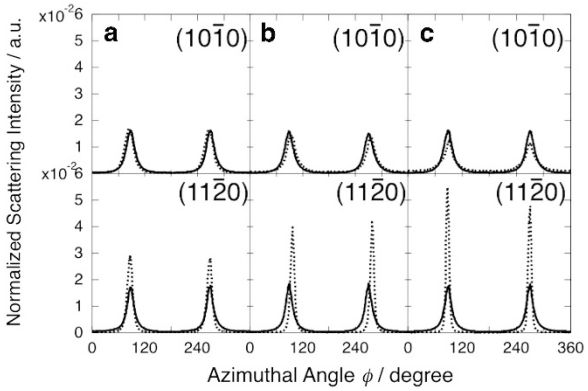

Figure 8 Dependency of intensity on azimuthal angle for $(10\bar{1}0)$ and $(11\bar{2}0)$ reflection peaks for (**a**) Hep-5/Hep-5a, (**b**) Hep-6/Hep-6a, (**c**) Hep-7/Hep-7a, where solid and dotted curves represent before and after the subsequent annealing, respectively.

To quantitatively discuss the extent of orientation for the $(11\bar{2}0)$ planes, the orientation factor is evaluated based on the azimuthal distribution of the scattering intensities shown in Figures 5 and 8. Namely, the second-order orientation factor F can be evaluated as

$$F = C^{-1}\frac{3\langle \cos^2\phi\rangle - 1}{2} \qquad (3)$$

where the constant C is attributed to the geometric relationship of the probe orientation (with angle Φ) with respect to the cylinder axis and

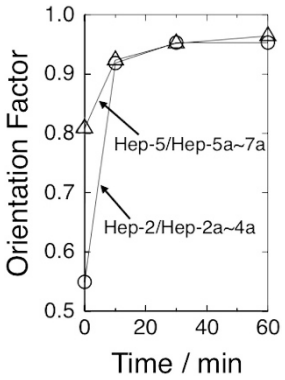

Figure 9 Orientation factor calculated using equation (3) for the dependency of intensity on azimuthal angle for the $(11\bar{2}0)$ reflection peaks for Hep-2/Hep-2a–4a (open circle) and Hep-5/Hep-5a–7a (open triangle).

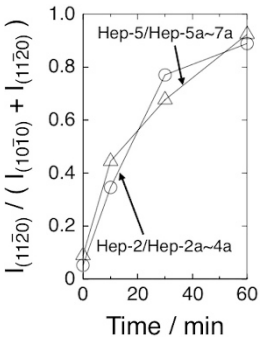

Figure 10 Fraction of peak-top intensity for the $(10\bar{1}0)$ and $(11\bar{2}0)$ reflection peaks appearing in the equatorial direction for Hep-2/Hep-2a–4a (open circle) and Hep-5/Hep-5a–7a (open triangle).

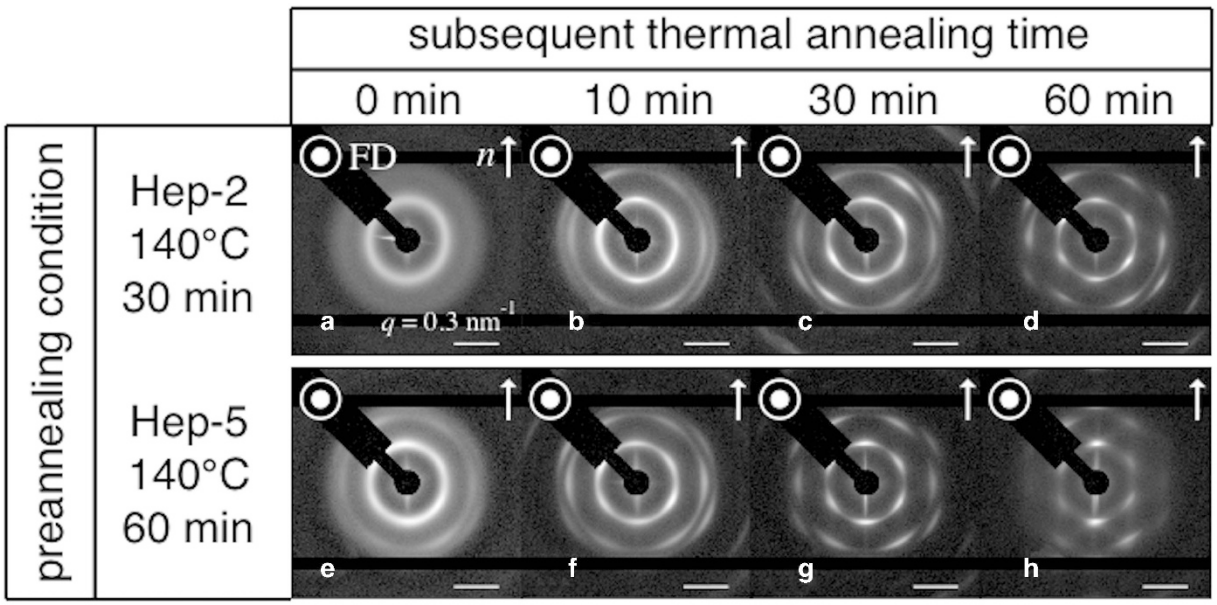

Figure 11 2d-SAXS patterns (end view) measured for (**a**–**d**) Hep-2/Hep-2a–4a and (**e**–**h**) Hep-5/Hep-5a–7a by X-ray irradiation parallel to FD and the specimen surface.

is given by

$$C = \frac{3\langle \cos^2\Phi \rangle - 1}{2} = -\frac{1}{2} \qquad \left(\Phi = \frac{\pi}{2}\right) \tag{4}$$

and

$$\langle \cos^2\phi \rangle = \frac{\int_0^{\pi} I(\phi) \cos^2\phi \sin\phi \, d\phi}{\int_0^{\pi} I(\phi) \sin\phi \, d\phi} \tag{5}$$

Note that $\langle \cos^2\phi \rangle = 0$ for a perfectly parallel orientation, thus $F = 1$, while $\langle \cos^2\phi \rangle = 1/3$, thus $F = 0$ for a random orientation. An axisymmetric orientation of cylinders with respect to FD was assumed, as shown schematically in Figure 1c. Figure 9 shows the changes in the evaluated orientation factor as a function of time for the subsequent annealing. As mentioned in the experimental procedure section, no load was applied to the specimen during the subsequent thermal annealing. Additionally, the plotted values at annealing time zero represent Hep-2 and Hep-5. The other plots reflect each specimen's orientation factor. The extent of orientation was found to be nearly identical, regardless of the initial state of orientation. Interestingly, the cylindrical orientation increased most rapidly within the first 10 min of thermal annealing (from Hep-2 to Hep-2a). This is surprising because no load was applied during thermal annealing. The spontaneous improvement of cylinder orientation by thermal annealing without an application of flow has been reported in the case of the perpendicular orientation for the same sample (SEBS-16).[19] This phenomenon is interpreted to be a grain-coarsening mechanism. Upon application of the load in the preannealing stage, some extent of cylinder orientation is obtained. The grains in which the cylinders are preferentially oriented parallel to FD are considered to be larger than grains with inclined cylinder orientation. As time elapses, the former grains will grow, while the latter grains shrink. A relatively large grain surrounded by smaller grains will grow preferentially. It may be anticipated that cylinder orientation in the grain would degrade upon growth of the grain; however, the results shown in Figure 9 demonstrate that the total orientation factor increased with further

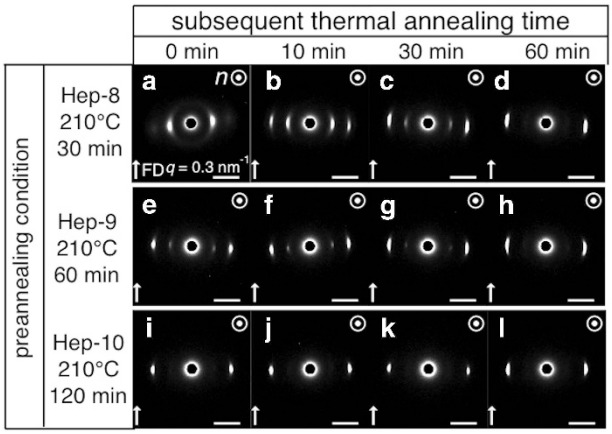

Figure 12 2d-SAXS patterns (through view) measured for (**a**–**d**) Hep-8/Hep-8a–8c, (**e**–**h**) Hep-9/Hep-9a–9c and (**i**–**l**) Hep-10/Hep-10a–10c.

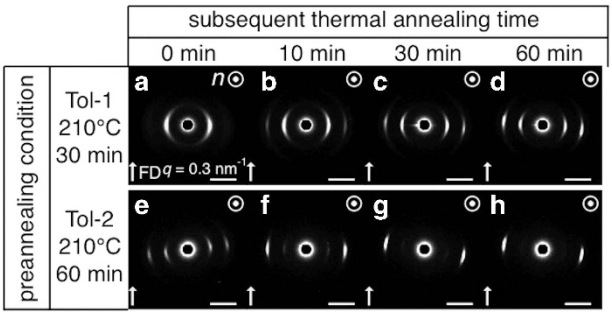

Figure 13 2d-SAXS patterns (through view) measured for (**a**–**d**) Tol-1/Tol-1a–1c and (**e**–**h**) Tol-2/Tol-2a–2c.

annealing (from 10 min to 60 min). This clearly indicates that the cylinder orientation in the grains improved. The mechanism of the spontaneous improvement of cylinder orientation is not clearly understood at present.

As discussed for Figures 4 and 7, it is implied that the fraction of the grains in which the $(10\bar{1}0)$ planes are parallel to the specimen surface increased as a function of the subsequent-annealing time. For a more quantitative examination, the fraction of peak-top intensity for the reflection peaks appearing in the equatorial direction, $I_{(11\bar{2}0)}/(I_{(10\bar{1}0)}+I_{(11\bar{2}0)})$, was plotted as a function of the subsequent-annealing time, as shown in Figure 10. It should be noted here that the fraction represents the grains in which not only the $(10\bar{1}0)$ planes are parallel to the specimen surface but also the cylinders in the grain were oriented perfectly parallel to FD. The behavior is similar for Hep-2/Hep-2a–4a and for Hep-5/Hep-5a–7a. Namely, the fraction of the grains in which the $(10\bar{1}0)$ planes were parallel to the specimen surface increased similarly, regardless of the initial orientational states in either Hep-2 or Hep-5. In contrast to Figure 9, Figure 10 shows a moderate increase as a function of time. Note that the value plotted in the ordinate of Figure 10 is the measure of orientation of the $(10\bar{1}0)$ planes parallel to the specimen surface. Therefore, it is concluded that the cylinder orientation and the $(10\bar{1}0)$ plane orientation do not occur concurrently. Furthermore, the tendency of the $I_{(11\bar{2}0)}/(I_{(10\bar{1}0)}+I_{(11\bar{2}0)})$ fraction to increase is moderate because of the two-step mechanism involved; first, cylinders are oriented parallel to the FD and then the grain orientation follows.

Figure 11 shows the changes in 2d-SAXS patterns (end view) as a function of time (for Hep-2/Hep-2a–4a and for Hep-5/Hep-5a–7a).

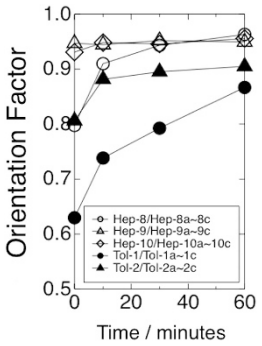

Figure 14 Subsequent annealing time dependencies of the orientation factor evaluated for Hep-8/Hep-8a–8c (open circle), Hep-9/Hep-9a–9c (open triangle), Hep-10/Hep-10a–10c (open diamond), Tol-1/Tol-1a–1c (filled circle) and Tol-2/Tol-2a–2c (filled triangle).

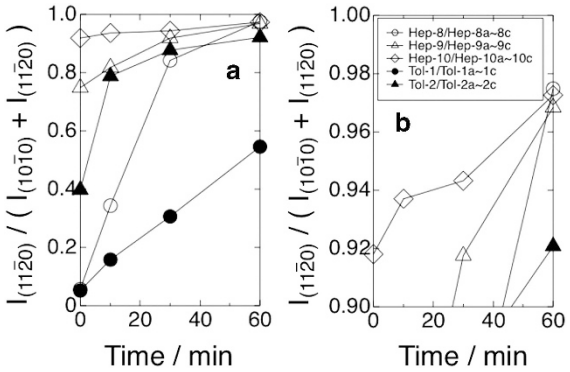

Figure 15 (**a**) Fraction of peak-top intensity for the $(10\bar{1}0)$ and $(11\bar{2}0)$ reflection peaks appearing in the equatorial direction for Hep-8/Hep-8a–8c (open circle), Hep-9/Hep-9a–9c (open triangle), Hep-10/Hep-10a–10c (open diamond), Tol-1/Tol-1a–1c (filled circle) and Tol-2/Tol-2a–2c (filled triangle). The expanded plot is shown in the **b**.

The 2d-SAXS patterns are depicted according to a gray scale of the logarithmic intensity. At time equal to zero, an isotropic SAXS pattern is observed in Figure 11, indicating that the $(10\bar{1}0)$ planes are not preferentially oriented. Over time, the 2d-SAXS pattern gradually changed into spotty hexagonal patterns. This clearly supports the conclusion discussed above that the $(10\bar{1}0)$ planes were oriented parallel to the specimen surface.

To examine the effect of the preannealing temperature, specimens were preannealed at a higher temperature (210 °C). Figure 12 shows a variety of 2d-SAXS patterns (through view) as a function of the subsequent–annealing time for (a) Hep-8, (e) Hep-9, and (i) Hep-10. Note that (b)–(d) are for Hep-8a–8c, (f)–(h) are for Hep-9a–9c, and (j)–(l) are for Hep-10a–10c, respectively. First of all, an appreciable cylinder orientation was already obtained for the specimens subjected to the preannealing at 210 °C, as compared with the specimens preannealed at 140 °C (see Figures 3 and 6). Furthermore, the 2d-SAXS pattern in Figure 12i lacks a first-order peak (the $(10\bar{1}0)$ reflection peak), which indicates not only a perfect cylinder orientation but also that the $(10\bar{1}0)$ plane orientation had proceeded during preannealing, without the subsequent annealing. This implies that the subsequent thermal annealing is not required for appreciable cylinder orientation.

To quantitatively evaluate these findings, the orientation factor and the fraction of the grains in which the $(10\bar{1}0)$ planes are parallel to the

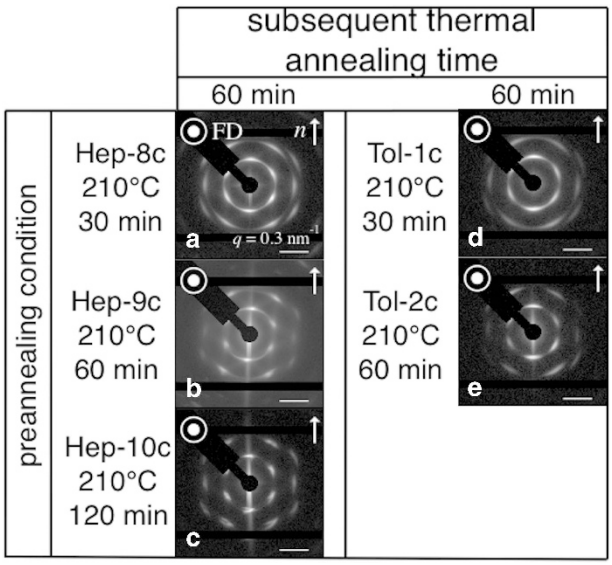

Figure 16 2d-SAXS patterns (end view) measured for (**a**–**c**) Hep-8c–10c, respectively, and (**d**,**e**) Tol-1c and 2c, respectively, by X-ray irradiation parallel to the FD and the specimen surface.

specimen surface are plotted as a function of the subsequent annealing in Figures 14 and 15, respectively. The effect of the initial morphology in the as-cast specimens was examined using Tol-1 and Tol-2, obtained by preannealing the as-cast specimens with cylinders formed directly by casting from the toluene solution. Figure 13 shows several 2d-SAXS patterns (through view) as a function of annealing time for (a) Tol-1 and (e) Tol-2. Note that (b)–(d) are for Tol-1a–1c, and (f)–(h) are for Tol-2a–2c, respectively. The cylindrical orientation for all samples cast from toluene solution are poor compared with those shown in Figures 12a–h. For a more quantitative analysis, the orientation factor and the fraction of the grains in which the $(10\bar{1}0)$ planes are parallel to the specimen surface are plotted together in Figures 14 and 15, respectively. The corresponding 1d-SAXS profiles for Figures 12 and 13 are shown in the supporting information in Supplementary Figures S2 and S3, respectively. Additionally, the dependency of intensity on azimuthal angle for the $(10\bar{1}0)$ and $(11\bar{2}0)$ reflection peaks is shown in the supporting information in Supplementary Figures S4 and S5, respectively.

The cylinder orientation and the increase in the fraction of the grains with $(10\bar{1}0)$ planes parallel to the specimen surface are discussed below. Although the orientation factor did not change as a function of time for Hep-9 (open triangle) and Hep-10 (open diamond), implying that the subsequent annealing was not needed, it was found in Figure 15b that the intensity fraction gradually increased as a function of time. Therefore, we conclude that the subsequent annealing is required to induce the most stable $(10\bar{1}0)$ plane orientation. After 60 min of the subsequent annealing, the orientation factor is almost identical to the factor for the Hep-8c, Hep-9c, and Hep-10c specimens, which also resembles the results for Hep-4a and Hep-7a (Figure 9). The fraction plotted in Figure 15 at 60 min of the subsequent annealing agrees with the values for Hep-8c, Hep-9c, and Hep-10c, but is slightly larger than for Hep-4a and Hep-7a (Figure 10). This clearly indicates the superiority of using a higher temperature in the preannealing step. Although the subsequent annealing of Tol-1 and Tol-2 improved the orientation of the cylinders and of the $(10\bar{1}0)$ plane, the smaller extent of cylinder orientation for Tol-1c and Tol-2c at 60 min of the subsequent annealing in Figure 14 clearly demonstrates the superiority of the sphere-coalescing method. Figure 16 shows the 2d-SAXS patterns (end view) measured for Hep-8c–10c, Tol-1c and Tol-2c. Similar to the results shown in Figure 11, these patterns clearly support the conclusion that the $(10\bar{1}0)$ planes were oriented parallel to the specimen surface.

CONCLUSION

To achieve highly oriented cylindrical morphology, we applied a compressional flow field with a slow deformation rate onto a SEBS-16 triblock copolymer film, causing a sphere-to-cylinder transition. After applying the flow, the specimen was further thermally annealed in the absence of an applied load. The resulting orientation of the cylindrical phase was analyzed by 2d-SAXS. The cylinder orientation parallel to FD was clearly seen to improve with an increase in the preannealing temperature and time. With subsequent thermal annealing, the cylinder orientation was found to rapidly improve within 10 min of annealing. However, no further increase in cylinder orientation was found for thermal annealing times longer than 30 min. For this time range, the fraction of the grains in which the $(10\bar{1}0)$ planes were parallel to the specimen surface gradually increased. The increase in the fraction qualitatively suggests that the cylinder orientation and the fraction of the grains with $(10\bar{1}0)$ planes parallel to the specimen surface are not concurrent events; the cylinders orient parallel to FD first. The preannealing condition at 210 °C for 120 min ($\varepsilon = 4.51$) and subsequent thermal annealing at 210 °C for 60 min was found to be the best condition for obtaining both superior cylinder orientation and an extremely high fraction of the aligned grains. The application of flow directly to a cylindrical morphology resulted in a lesser degree of cylinder orientation than by transforming spheres to cylinders. This indicates the superiority of utilizing the coalescence of spheres for achieving cylindrical orientation via application of flow.

CONFLICT OF INTEREST

The authors declare no conflict of interest.

ACKNOWLEDGEMENTS

This study was partially supported by the Grant-in-Aid for Scientific Research on Innovative Areas, 'New Polymeric Materials Based on Element-Blocks' (No. 25102524), from the Ministry of Education, Culture, Sports, Science, and Technology of Japan.

1 Helfand, E. Block copolymer theory. III. statistical mechanics of the microdomain structure. *Macromolecules* **8**, 552–556 (1975).
2 Helfand, E. & Wasserman, Z. R. Block copolymer theory. 6. Cylindrical domains. *Macromolecules* **13**, 994–998 (1980).
3 Vavasour, J. D. & Whitmore, M. D. Self-consistent field theory of block copolymers with conformational asymmetry. *Macromolecules* **26**, 7070–7075 (1993).
4 Matsen, M. W. & Bates, F. S. Unifying weak- and strong-segregation block copolymer theories. *Macromolecules* **29**, 1091–1098 (1996).
5 Sakamoto, N., Hashimoto, T., Han, C. D. & Vaidya, D. K. N. Y. Order-order and order-disorder transitions in a polystyrene-block-polyisoprene-block-polystyrene copolymer. *Macromolecules* **30**, 1621–1632 (1997).
6 Matsen, M. W. & Thompson, R. B. Equilibrium behavior of symmetric ABA triblock copolymer melts. *J. Chem. Phys.* **111**, 7139 (1999).
7 Kimishima, K., Koga, T. & Hashimoto, T. Order-order phase transition between spherical and cylindrical microdomain structures of block copolymer. I. Mechanism of the transition. *Macromolecules* **33**, 968–977 (2000).
8 Sota, N., Saijo, K., Hasegawa, H., Hashimoto, T., Amemiya, Y. & Ito, K. Directed self-assembly of block copolymers into twin bcc-sphere: phase transition process from aligned hex-cylinder to bcc-sphere induced by a temperature jump between the two equilibrium phases. *Macromolecules* **46**, 2298–2316 (2013).
9 Cohen, R. E. & Bates, F. S. Nonequilibrium morphologies of a diblock copolymer of polyisoprene and poly(*n*-butyl methacrylate). *J. Polym. Sci. Part B Polym. Phys.* **18**, 2143–2148 (1980).

10 Shibayama, M., Hashimoto, T. & Kawai, H. Ordered structure in block polymer solutions. 1. Selective solvents. *Macromolecules* **16**, 16–28 (1983).
11 Hajduk, D. A., Gruner, S. M., Rangarajan, P., Register, R. A., Fetters, L. J., Honeker, C., Albalak, R. J. & Thomas, E. L. Observation of a reversible thermotropic order-order transition in a diblock copolymer. *Macromolecules* **27**, 490–501 (1994).
12 Sakurai, S., Umeda, H., Taie, K. & Nomura, S. Kinetics of morphological transition in polystyrene-*block*-polybutadiene-*block*-polystyrene triblock copolymer melt. *J. Chem. Phys.* **105**, 8902 (1996).
13 Funaki, Y., Kumano, K., Nakao, T., Jinnai, H., Yoshida, H., Kimishima, K., Tsutsumi, K., Hirokawa, Y. & Hashimoto, T. Influence of casting solvents on microphase-separated structures of poly(2-vinylpyridine)-*block*-polyisoprene. *Polymer* **40**, 7147–7156 (1999).
14 Morkved, T. L., Lu, M., Urbas, A. M., Ehrichs, E. E., Jaeger, H. M., Mansky, P. & Russell, T. P. Local control of microdomain orientation in diblock copolymer thin films with electric fields. *Science* **273**, 931–933 (1996).
15 Thurn-Albrecht, T., Schotter, J., Kastle, G. A., Emley, N., Shibauchi, T., Krusin-Elbaum, L., Guarini, K., Black, C. T., Tuominen, M. T. & Russell, T. P. Ultrahigh-density nanowire arrays grown in self-assembled diblock copolymer templates. *Science* **290**, 2126–2129 (2000).
16 Kim, S. H., Misner, M. J., Xu, T., Kimura, M. & Russell, T. P. Highly oriented and ordered arrays from block copolymers via solvent evaporation. *Adv. Mater.* **16**, 226–231 (2004).
17 Xu, T., Zvelindovsky, A. V., Sevink, G. J. A., Gang, O., Ocko, B., Zhu, Y., Gido, S. P. & Russell, T. P. Electric field induced sphere-to-cylinder transition in diblock copolymer thin films. *Macromolecules* **37**, 6980–6984 (2004).
18 Cavicchi, K. A., Berthiaume, K. J. & Russell, T. P. Solvent annealing thin films of poly (isoprene-*b*-lactide). *Polymer* **46**, 11635–11639 (2005).
19 Sakurai, S., Bando, H., Yoshida, H., Fukuoka, R., Mouri, M., Yamamoto, K. & Okamoto, S. Spontaneous perpendicular orientation of cylindrical microdomains in a block copolymer thick film. *Macromolecules* **42**, 2115–2121 (2009).
20 Singh, G., Yager, K. G., Smilgies, D.-M., Kulkarni, M. M., Bucknall, D. G. & Karim, A. Tuning molecular relaxation for vertical orientation in cylindrical block copolymer films via sharp dynamic zone annealing. *Macromolecules* **45**, 7107–7117 (2012).
21 Xue, J., Singh, G., Qiang, Z., Karim, A. & Vogt, B. D. Unidirectional self-assembly of soft templated mesoporous carbons by zone annealing. *Nanoscale* **5**, 7928–7935 (2013).
22 Singh, G., Batra, S., Zhang, R., Yuan, H., Yager, K. G., Cakmak, M., Berry, B. & Karim, A. Large-scale roll-to-roll fabrication of vertically oriented block copolymer thin films. *ACS Nano* **7**, 5291–5299 (2013).
23 Yin, J., Yao, X., Liou, J.-Y., Sun, W., Sun, Y-S. & Wang, Y. Membranes with highly ordered straight nanopores by selective swelling of fast perpendicularly aligned block copolymers. *ACS Nano* **7**, 9961–9974 (2013).
24 Mansky, P., Harrison, C. K., Chaikin, P. M., Register, R. A. & Yao, N. Nanolithographic templates from diblock copolymer thin films. *App. Phys. Lett.* **68**, 2586 (1996).
25 Lee, H. H., Register, R. A., Hajduk, D. A. & Gruner, S. M. Orientation of triblock copolymers in planar extension. *Polym. Eng. Sci.* **36**, 1414–1424 (1996).
26 Daniel, C., Hamley, I. W. & Mortensen, K. Effect of planar extension on the structure and mechanical properties of polystyrene–poly(ethylene-*co*-butylene)-polystyrene triblock copolymers. *Polymer* **41**, 9239–9247 (2000).
27 Villar, M. A., Rueda, D. R., Ania, F. & Thomas, E. L. Study of oriented block copolymers flms obtained by roll-casting. *Polymer* **43**, 5139–5145 (2002).
28 Stasiak, J., Squires, A. M., Castelletto, V., Hamley, I. W. & Moggridge, G. D. Effect of stretching on the structure of cylinder- and sphere-forming styrene – isoprene – styrene block copolymers. *Macromolecules* **42**, 5256–5265 (2009).
29 Folkes, M. J., Keller, A. & Scalisi, F. P. An extrusion technique for the preparation of 'single-crystals' of block copolymers. *Colloid. Polym. Sci.* **251**, 1–4 (1973).
30 Morrison, F. A. & Winter, H. H. Effect of unidirectional shear on the structure of triblock copolymers. 1. polystyrene-polybutadiene-polystyrene. *Macromolecules* **22**, 3533–3540 (1989).
31 Morrison, F. A., Winter, H. H., Gronski, W. & Barnes, J. D. Effect of unidirectional shear on the structure of triblock copolymers. 2. polystyrene-polyisoprene-polystyrene. *Macromolecules* **23**, 4200–4205 (1990).
32 Scott, D. B., Waddon, A. J., Lin, Y.-G., Karasz, F. E. & Winter, H. H. Shear-induced orientation transitions in triblock copolymer styrene-butadiene-styrene with cylindrical domain morphology. *Macromolecules* **25**, 4175–4181 (1992).
33 Okamoto, S., Saijo, K. & Hashimoto, T. Real-time SAXS observations of lamella-forming block copolymers under large oscillatory shear deformation. *Macromolecules* **27**, 5547–5555 (1994).
34 Zhang, Y., Wiesner, U. & Spiess, H. W. Frequency dependence of orientation in dynamically sheared diblock copolymers. *Macromolecules* **28**, 778–781 (1995).
35 Angelescu, D. E., Waller, J. H., Adamson, D. H., Deshpande, P., Chou, S. Y., Register, R. A. & Chaikin, P. M. Macroscopic orientation of block copolymer cylinders in single-layer films by shearing. *Adv. Mater.* **16**, 1736–1740 (2004).
36 Davis, R. L., Chaikin, P. M. & Register, R. A. Cylinder orientation and shear alignment in thin films of polystyrene–poly(*n*-hexyl methacrylate) diblock copolymers. *Macromolecules* **47**, 5277–5285 (2014).
37 Sakurai, S., Kota, T., Isobe, D., Okamoto, S., Sakurai, K., Ono, T., Imaizumi, K. & Nomura, S. Synchrotron small-angle X-ray scattering studies on flow-induced gyroid to cylinder transition in an elastomeric SBS triblock copolymer. *J. Macromol. Sci. B* **43**, 1–11 (2004).
38 Khan, S. A. & Larson, R. G. Step planar extension of polymer melts using a lubricated channel. *Rheo. Acta* **30**, 1–6 (1991).
39 Morrison, F. A., Mays, J. W., Muthukumar, M., Nakatani, A. I. & Han, C. C. Shear-induced morphological structures in triblock copolymers. *Macromolecules* **26**, 5271–5273 (1993).

Supplementary Information accompanies the paper on Polymer Journal website (http://www.nature.com/pj)